Appendix S1

Assessing the effectiveness of vegetation indices in detecting forest disturbances in the southeast Amazon

Eduardo Q. Marques[a,b,c,*], Divino V. Silvério[a,c], Lenio S. Galvão[d], Luiz E. O. C. Aragão[d], Maria R. Uribe[e], Marcia N. Macedo[b,f], Ludmila Rattis[b,f], Ane A. C. Alencar[b], Paulo M. Brando[b,e]

[a]Universidade do Estado de Mato Grosso, Nova Xavantina, MT, Brazil
[b]Instituto de Pesquisa Ambiental da Amazônia, Brasília, DF, Brazil
[c]Universidade Federal Rural da Amazônia, Capitão Poço, PA, Brazil
[d]Instituto Nacional de Pesquisas Espaciais, São José dos Campos, SP, Brazil
[e]Yale School of the Environment, Yale University, Yale, CT, USA
[f]Woodwell Climate Research Center, Falmouth, MA, USA

*Corresponding author.
E-mail address: eduardo.marques@unemat.br (E.Q. Marques)

Section S1

Detailed material and methods

Study area

Our study area is in the municipality of Querência (Mato Grosso state) in the southeastern portion of the Amazon Basin (13°04′35.39” S, 52°23′08.85” W). The climate of the region is tropical with a dry winter (Aw), according to the Köppen classification, with well-defined dry (May to September) and rainy (October to April) periods [1]. The experimental area was described in detail by Balch et al. (2008) [2]. Briefly, the experimental area comprised three adjacent plots of 50 ha each, each subject to different burning regimes: an unburned (Control), a plot burned every year (B1yr), and a plot burned every three years (B3yr) from 2004-2010, except for 2008. During this period, the B3yr and B1yr plots were burned three and six times, respectively [3]. All plots have been monitored continuously since the last fire in 2010 to track forest recovery over time.

Landsat datasets and VIs

We used 45 TM/Landsat-5 images and 22 OLI/Landsat-8 images obtained during the local dry season (June and August) between 1985 and 2019. We restricted images to this fixed time range to reduce potentially confounding effects of changing solar illumination and vegetation seasonality, particularly for the VIs most sensitive to forest degradation. The Landsat images downloaded from the United States Geological Survey (USGS) were pre-processed to surface reflectance after undergoing atmospheric and geometric corrections. Using the Landsat datasets, we selected six VIs to represent multispectral changes with fire in vegetation structure and biochemistry: the Enhanced Vegetation Index (EVI), Normalized Difference Vegetation Index (NDVI), Green-Red Normalized Difference (GRND), Normalized Difference Infrared Index (NDII), Normalized Burn Ratio (NBR), and the Normalized Burn Ratio 2 (NBR2). Equations and references of these VIs are shown in Table S1.

EVI is essentially a structural index, given its dependence on near-infrared reflectance (NIR) [4,5]. NDVI is the most traditional VI and is equally dependent on NIR and red reflectance [6]. GRND was selected because of its sensitivity to new foliage [7], whereas NDII was chosen to track eventual changes in moisture stress of vegetation [8]. Finally, NBR and NBR2 are VIs generally used to study burned areas, taking advantage of spectral changes associated with vegetation structure in the NIR and vegetation moisture in the shortwave infrared (SWIR-1 and SWIR-2 intervals) [9,10]. To calculate these VIs, we used the R statistical environment [11] and the raster package [12].

Table S1. Vegetation indices calculated from multispectral bands of the TM/Landsat-5 and OLI/Landsat-8 sensors, along with their respective equations and references.

Vegetation Index	Equations	Reference
	Structure	
Enhanced Vegetation Index (EVI)	2.5 × ((ρ830nm − ρ660nm) / (ρ830nm + 6 × ρ660nm − 7.5 × ρ485nm + 1))	Huete *et al* 2002
Normalized Difference Vegetation Index (NDVI)	(ρ830nm − ρ660nm) / (ρ830nm + ρ660nm)	Rouse *et al* 1973
Green-Red Normalized Difference (GRND)	(ρ560nm − ρ660nm) / (ρ560nm + ρ660nm)	de Moura *et al* 2017
	Biochemistry	
Normalized Difference Infrared Index (NDII)	(ρ830nm − ρ1650nm) / (ρ830nm + ρ1650nm)	Hunt and Rock 1989
	Fire, structure, vegetation moisture	
Normalized Burn Ratio (NBR)	(ρ830nm − ρ2215nm) / (ρ830nm + ρ2215nm)	García and Caselles 1991
Normalized Burn Ratio 2 (NBR2)	(ρ1650nm – ρ2215nm) / (ρ1650nm + ρ2215nm)	van Deventer *et al* 1997

Hyperion/EO-1 and VIs

We used Hyperion/EO-1 data to calculate 17 narrowband VIs and evaluate their sensitivity to detect forest degradation caused by the experimental fire. We downloaded the L1R data from the USGS for the local dry season (June-August) from 2004 to 2012. Nadir-viewing observations were not available for 2007 and 2009.

Hyperion image pre-processing included four main steps before calculating the VIs. First, we reduced the striping effects by replacing abnormal vertical columns with the average response of the adjacent columns in each band image. Second, we converted the radiance data into surface reflectance images using the Fast Line-of-sight Atmospheric Analysis of Spectral Hypercubes (FLAASH) algorithm. FLAASH is based on the MODTRAN radiative transfer model [18,19]. Here, we used a tropical atmosphere with a rural aerosol model, and estimated the visibility using the 2-Band (K–T) method [20], Third, we excluded bands around 1400 nm and 1900 nm from subsequent data analyses due to the strong atmospheric absorption by water vapor, which limits the utility of these data even after atmospheric correction [21]. In total, we retained 146 spectral bands in the subsequent processes and analyses. Finally, we geometrically corrected the Hyperion images in the QGIS 3.2.2 software [22], using control points on corresponding features between the Hyperion images and an orthorectified Landsat 5 image. We adopted the UTM zone 22S projection system, WGS-84 datum for all data layers.

After image pre-processing, we calculated the 17 narrowband VIs listed in Table S2. They were selected carefully to represent vegetation structure [*EVI, NDVI, Visible Atmospherically Resistant Index (VARI), and Visible Index Green (VIG)*]; biochemistry [*Leaf Water Vegetation Index 2 (LWVI2), Moisture Stress Index (MSI), NDII, Normalized Difference Water Index (NDWI), Pigment Specific Simple Ratio (PSSR), Plant Senescence Reflectance Index (PSRI), Structure Insensitive Pigment Index (SIPI), Water Band Index (WBI), and Near-Infrared Reflectance of Vegetation (NIRv)*]; and physiology [*Photochemical Reflectance Index (PRI), and Red Edge NDVI (RENDVI)*]. Some of them are sensitive to more than one vegetation parameter [23]. As with Landsat, NBR and NBR2 are often used in specific studies of burned areas.

Table S2. Vegetation indices calculated from Hyperion/EO-1 data, with their respective formulas and references.

Vegetation Index	Equations	Reference
	Structure	
Enhanced Vegetation Index (EVI)	2.5 × ((ρ864nm − ρ660nm) / (ρ864nm + 6 × ρ660nm − 7.5 × ρ467nm + 1))	Huete *et al* 2002
Normalized Difference Vegetation Index (NDVI)	(ρ864nm − ρ660nm) / (ρ864nm + ρ660nm)	Rouse *et al* 1973
Visible Atmospherically Resistant Index (VARI)	(ρ559nm − ρ660nm) / (ρ559nm + ρ660nm - ρ487nm)	Gitelson *et al* 2002
Visible Index Green (VIG)	(ρ559nm − ρ660nm) / (ρ559nm + ρ660nm)	Gitelson *et al* 2002
	Biochemistry	
Leaf Water Vegetation Index 2 (LWVI2)	(ρ1094nm – ρ1205nm) / (ρ1094nm + ρ1205nm)	Galvão *et al* 2005
Moisture Stress Index (MSI)	(ρ1598nm) / (ρ823nm)	Hunt and Rock 1989
Normalized Difference Infrared Index (NDII)	(ρ823nm − ρ1649nm) / (ρ823nm + ρ1649nm)	Hunt and Rock 1989
Normalized Difference Water Index (NDWI)	(ρ854nm − ρ1245nm) / (ρ854nm + ρ1245nm)	Gao 1996
Pigment Specific Simple Ratio (PSSR)	ρ803nm / ρ671nm	Blackburn 1998
Plant Senescence Reflectance Index (PSRI)	(ρ681nm - ρ498nm) / ρ752nm	Merzlyak *et al* 1999
Structure Insensitive Pigment Index (SIPI)	(ρ803nm − ρ467nm) / (ρ803nm + ρ681nm)	Penuelas *et al* 1995
Water Band Index (WBI)	ρ905nm / ρ972nm	Penuelas *et al* 1997
Near-Infrared Reflectance of Vegetation (NIRv)	P864nm x ((ρ864nm − ρ660nm) / (ρ864nm + ρ660nm))	Badgley *et al* 2017
	Physiology	
Photochemical Reflectance Index (PRI)	(ρ529nm − ρ569nm) / (ρ529nm + ρ569nm)	Gamon *et al* 1997

Red Edge NDVI (RENDVI)	(ρ752nm − ρ701nm) / (ρ752nm + ρ701nm)	Gitelson *et al* 1996
	Fire, structure, vegetation moisture	
Normalized Burn Ratio (NBR)	(ρ823nm − ρ1245nm) / (ρ823nm + ρ1245nm)	García and Caselles 1991
Normalized Burn Ratio 2 (NBR2)	(ρ1245nm − ρ1649nm) / (ρ1245nm + ρ1649nm)	van Deventer *et al* 1997

Field data

Forest inventories were carried out in pre-, during, and post-fire disturbance events to quantify tree mortality, biodiversity, and biomass stocks in the fire experimental area [2]. In each 50-ha treatment plot, all trees with diameter at breast height (DBH) ≥40 cm were measured (~930 individuals per plot). For trees and lianas with 20–40 cm DBH, we established six transects parallel to the forest edge, moving inward from the agricultural field at 10, 30, 100, 250, 500, and 750 meters from the edge (500 × 20 m; 5.5 ha sampled per treatment plot; ~ 880 individuals per plot). We also performed nested subsampling within these transects to measure trees and lianas with 10–20 cm DBH (500 × 4 m; 1.2 ha sampled per treatment plot; ~490 individuals per plot). These inventories were repeated annually on each 50-ha plot [2] and used to estimate above-ground biomass (ABG) based on an allometric equation calibrated for tropical dry forests, which estimates tree biomass based on DBH, wood density, and height [34].

Leaf Area Index (LAI) was measured in the field at 200 different points per plot from 2005 to 2017 and used to evaluate the correlation with satellite-based VIs. To measure LAI, two LiCor 2000 sensors (LI-COR Biosciences Inc, Lincoln) were used. One instrument was placed in an adjacent open field to measure incoming radiation without canopy influence, while the other instrument was used simultaneously to perform measurements inside the forest. The light field of each sensor was reduced to 90% using opaque caps. The two instruments were intercalibrated before each set of field measurements. All measurements were standardized to 1-m height from the ground and for diffused light conditions before 8:00 am or after 5:00 pm [35].

As a proxy for forest productivity, we estimated biweekly litterfall production using 210 baskets (70 per plot, 0.5 m² each) placed systematically throughout the plots to measure litter production from August 2004 to August 2018. The baskets were placed 1-m above the forest floor and woody debris (>1 cm) was removed at the time of collection. The litter samples were dried in the oven for 48 hours (at 70°C) to obtain the dry mass, which was measured using a balance with an accuracy of 0.01g.

Data analysis

To assess the efficacy of each VI in detecting post-fire vegetation changes, we calculated the percentage spectral change over the study area. The efficacy of each VI in detecting fire-associated changes was calculated as the difference between the values in the burned plots (B1yr and B3yr) and the Control plot, and then standardized as a percentage. We then evaluated the uncertainties by calculating 95% confidence intervals based on the 'Z' distribution test to compare across the treatments. To evaluate the variability of the multispectral VIs over time and the differences between treatments, we generated a simple model of temporal change by employing the Loess method as implemented in the *geom_smooth* function of the R package *ggplot2* [36]. We also incorporated the standard errors (SE), calculated based on the Loess methods, to better assess the model's precision and improve confidence in its predictions[37]. For the hyperspectral VIs, we employed the same method to evaluate the differences between plots; however, the analysis was restricted to the indices that showed the strongest responses to forest disturbances. To evaluate vegetation response to edge effects, we compared the responses of multispectral and hyperspectral VIs at the forest edge (first 250 m) to the forest interior (>250 m from the edge) of the experimental plot.

To assess how hyperspectral images improve our ability to map and understand forest degradation, we performed Principal Component Analyses (PCA) for the entire hyperspectral time series (2004–2012) and for individual years, allowing us to identify patterns of vegetation change throughout the fire experiment. For annual PCAs, we compared the pre-experiment (2004) and post-experiment (2012) periods. We then used eigenvectors to evaluate the relative contribution of each VI to the explanation of a given component. We also compared the results of the 17 hyperspectral VIs with those of the six multispectral VIs using Pearson's correlation coefficients to develop a correlation matrix, which enabled us to verify which hyperspectral VIs were mostly correlated with the multispectral VIs (≥0.9).

To evaluate the effectiveness of hyperspectral and multispectral VIs in detecting changes in forest disturbance, we first evaluated the eight VIs most sensitive to changes associated with fire, calculated as the maximum difference between burned (B1yr and B3yr) and the Control plot during the fire period, followed by a Linear Model (LM). In these models, we used three variables measured *in situ* as response variables: biomass, litterfall, and LAI. As predictors, we selected four VIs derived from Landsat (GRND, EVI, NBR, and NDII) and four derived from

Hyperion (PRSI, VARI, MSI, and VIG) that were most responsive to changes associated with fire (see Fig. 3 and 4). We present the results for the most sensitive VI derived from Landsat (GRND) and Hyperion (PSRI) in the main text (Fig. 9), and the other six VIs are presented in the supplementary information (Fig. S8, S9, and S10).

We also modeled temporal changes in field data (biomass, litterfall, and LAI), as predicted by the VIs most sensitive to fire-related changes. To this end, we applied the loess smoothing method to visualize temporal trends using the *geom_smooth* function in the *ggplot2* R package[36]. Using the differences between the burned and Control treatments for each VI, we estimated the time required for vegetation to recover to the pre-fire baseline values.

References

1. Alvares, C. A., Stape, J. L., Sentelhas, P. C., De Moraes Gonçalves, J. L. & Sparovek, G. Köppen's climate classification map for Brazil. *metz* **22**, 711–728 (2013).
2. Balch, J. R. K. *et al.* Negative fire feedback in a transitional forest of southeastern Amazonia. *Global Change Biology* **14**, 2276–2287 (2008).
3. Brando, P. M. *et al.* Legacies of multiple disturbances on fruit and seed patterns in Amazonia: Implications for forest functional traits. *Ecosphere* **15**, e4780 (2024).
4. Huete, A. *et al.* Overview of the radiometric and biophysical performance of the MODIS vegetation indices. *Remote Sensing of Environment* **83**, 195–213 (2002).
5. Galvão, L. S. *et al.* On intra-annual EVI variability in the dry season of tropical forest: A case study with MODIS and hyperspectral data. *Remote Sensing of Environment* **115**, 2350–2359 (2011).
6. Rouse, J. W., Haas, R. H., Schell, J. A. & Deering, D. W. Monitoring vegetation systems in the Great Plains with ERTS. in *Proc. Third ERTS-1 Symp.* vol. 1 309–317 (NASA, Washington, DC, 1973).
7. de Moura, Y. M. *et al.* Spectral analysis of amazon canopy phenology during the dry season using a tower hyperspectral camera and modis observations. *ISPRS Journal of Photogrammetry and Remote Sensing* **131**, 52–64 (2017).
8. Hunt, E. & Rock, B. Detection of changes in leaf water content using Near- and Middle-Infrared reflectances☆. *Remote Sensing of Environment* **30**, 43–54 (1989).

9. García, M. J. L. & Caselles, V. Mapping burns and natural reforestation using thematic Mapper data. *Geocarto International* **6**, 31–37 (1991).
10. Van Deventer, A. P., Ward, A. D., Gowda, P. M. & Lyon, J. G. Using thematic mapper data to identify contrasting soil plains and tillage practices. *Photogrammetric Engineering and Remote Sensing* **63**, 87–93 (1997).
11. Core Team R Development. R: A language and environment for statistical computing. *R Foundation for Statistical Computing* http://www.r-project.org/. (2017).
12. Hijmans, R. J. *et al.* raster: Geographic analysis and modeling with raster data. Preprint at (2014).
13. Huete, A. *et al.* Overview of the radiometric and biophysical performance of the MODIS vegetation indices. *Remote Sensing of Environment* **83**, 195–213 (2002).
14. Rouse, W., Haas, R. H. & Deering, W. MONITORING THE VERNAL ADVANCEMENT AND RETROGRADATION (GREEN WAVE EFFECT) OF NATURAL VEGETATION.
15. Huntjr, E. & Rock, B. Detection of changes in leaf water content using Near- and Middle-Infrared reflectances☆. *Remote Sensing of Environment* **30**, 43–54 (1989).
16. García, M. J. L. & Caselles, V. Mapping burns and natural reforestation using thematic Mapper data. *Geocarto International* **6**, 31–37 (1991).
17. van Deventer, A. P., Ward, A. D., Gowda, P. H. & Lyon, J. G. Using Thematic Mapper Data to Identify Contrasting Soil Plains and Tillage Practices. (1997).
18. Felde, G. W. *et al.* Analysis of Hyperion data with the FLAASH atmospheric correction algorithm. in *IGARSS 2003. 2003 IEEE International Geoscience and Remote Sensing Symposium. Proceedings (IEEE Cat. No.03CH37477)* vol. 1 90–92 (IEEE).
19. Galvão, L. S., Roberts, D. A., Formaggio, A. R., Numata, I. & Breunig, F. M. View angle effects on the discrimination of soybean varieties and on the relationships between vegetation indices and yield using off-nadir Hyperion data. *Remote Sensing of Environment* **113**, 846–856 (2009).
20. Kaufman, Y. J. *et al.* Operational remote sensing of tropospheric aerosol over land from EOS moderate resolution imaging spectroradiometer. *Journal of Geophysical Research: Atmospheres* **102**, 17051–17067 (1997).

21. Galvão, L. S., Formaggio, A. R. & Tisot, D. A. Discrimination of sugarcane varieties in Southeastern Brazil with EO-1 Hyperion data. *Remote Sensing of Environment* **94**, 523–534 (2005).
22. Team, Q. D. QGIS Geographic Information System. Preprint at (2021).
23. Roberts, D. A., K. L. Roth, and R. L. P. Hyperspectral Vegetation Indices. in *Hyperspectral Remote Sensing of Vegetation* (ed. P. S. Thenkabail, J. G. Lyon, and A. H.) 309–327 (FL: CRC Press, Taylor and Francis Group, 2012).
24. Gitelson, A. A., Kaufman, Y. J., Stark, R. & Rundquist, D. Novel algorithms for remote estimation of vegetation fraction. *Remote Sensing of Environment* **80**, 76–87 (2002).
25. Galvão, L. S., Formaggio, A. R. & Tisot, D. A. Discrimination of sugarcane varieties in Southeastern Brazil with EO-1 Hyperion data. *Remote Sensing of Environment* **94**, 523–534 (2005).
26. Gao, B. NDWI—A normalized difference water index for remote sensing of vegetation liquid water from space. *Remote Sensing of Environment* **58**, 257–266 (1996).
27. Blackburn, G. A. Quantifying Chlorophylls and Caroteniods at Leaf and Canopy Scales: An Evaluation of Some Hyperspectral Approaches.
28. Merzlyak, M. N., Gitelson, A. A., Chivkunova, O. B. & Rakitin, V. Yu. Non-destructive optical detection of pigment changes during leaf senescence and fruit ripening. *Physiologia Plantarum* **106**, 135–141 (1999).
29. Penuelas, J., Frederic, B. & Filella, I. Semi-Empirical Indices to Assess Carotenoids/Chlorophyll-a Ratio from Leaf Spectral Reflectance. *Photosynthetica* **31**, 221–230 (1995).
30. Penuelas, J., Pinol, J., Ogaya, R. & Filella, I. Estimation of plant water concentration by the reflectance Water Index WI (R900/R970). *International Journal of Remote Sensing* **18**, 2869–2875 (1997).
31. Badgley, G., Field, C. B. & Berry, J. A. Canopy near-infrared reflectance and terrestrial photosynthesis. *Sci. Adv.* **3**, e1602244 (2017).
32. Gamon, J. A., Serrano, L. & Surfus, J. S. The photochemical reflectance index: an optical indicator of photosynthetic radiation use efficiency across species, functional types, and nutrient levels. *Oecologia* **112**, 492–501 (1997).

33. Gitelson, A. A., Merzlyak, M. N. & Lichtenthaler, H. K. Detection of Red Edge Position and Chlorophyll Content by Reflectance Measurements Near 700 nm. *Journal of Plant Physiology* **148**, 501–508 (1996).
34. Chave, J. *et al.* Improved allometric models to estimate the aboveground biomass of tropical trees. *Global Change Biology* **20**, 3177–3190 (2014).
35. Brando, P. M. *et al.* Prolonged tropical forest degradation due to compounding disturbances: Implications for CO2 and H2O fluxes. *Global Change Biology* 1–14 (2019) doi:10.1111/gcb.14659.
36. Wickham, H. Getting Started with ggplot2. in *ggplot2* 11–31 (Springer International Publishing, Cham, 2016). doi:10.1007/978-3-319-24277-4_2.
37. Cleveland, W. S. & Devlin, S. J. Locally Weighted Regression: An Approach to Regression Analysis by Local Fitting. *Journal of the American Statistical Association* **83**, 596–610 (1988).

Section S2

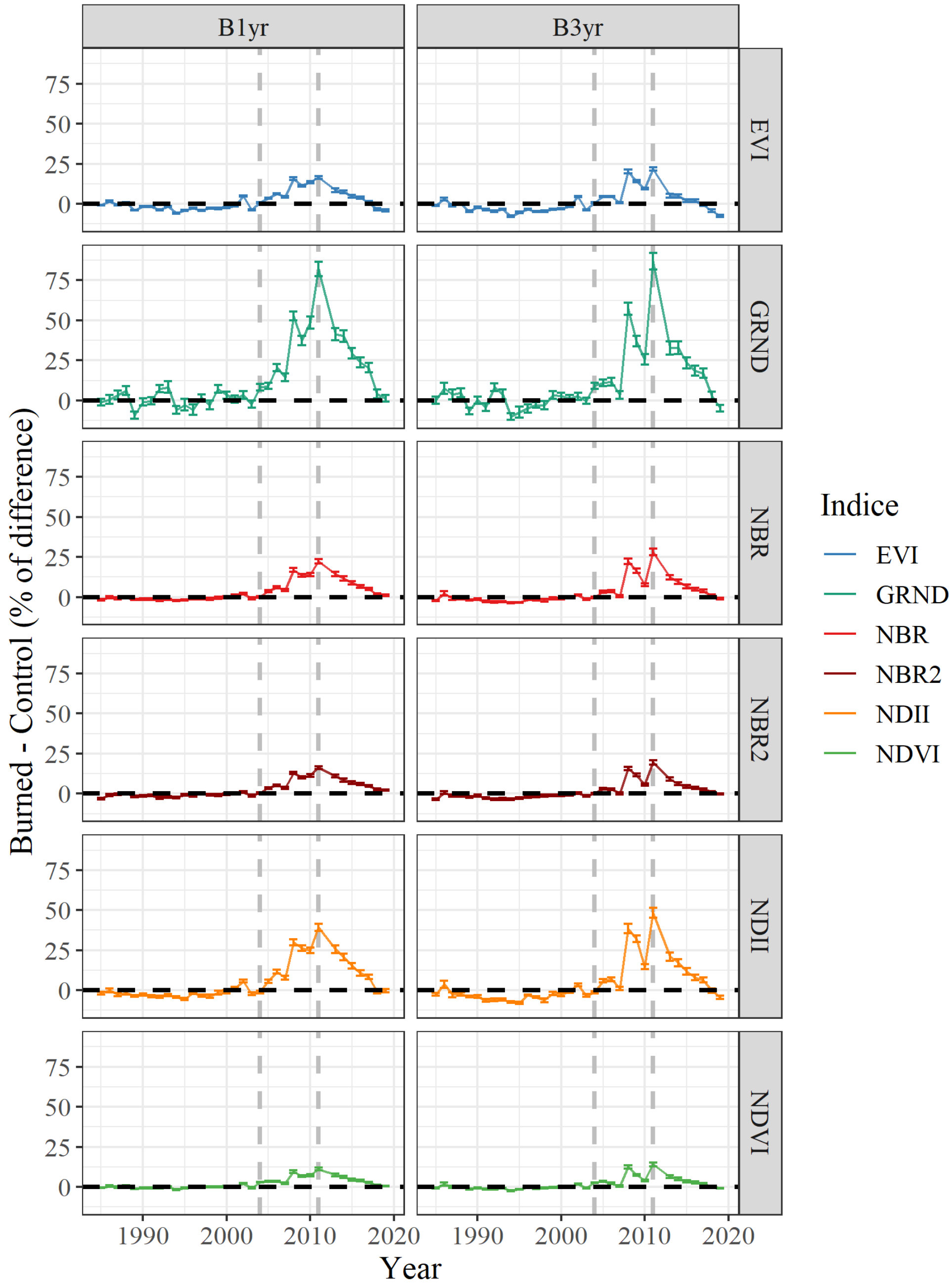

Figure S1. Relative difference in the means of the multispectral vegetation indices (Landsat) between the treatments burned every three years (B3yr), annually (B1yr), and the Control treatment. The values indicate the percentage change in relation to the Control treatment. The error bar indicates the 95% confidence intervals between burned treatments and Control mean. The dashed lines indicate the years in which the experimental fires were conducted (2004 to 2010).

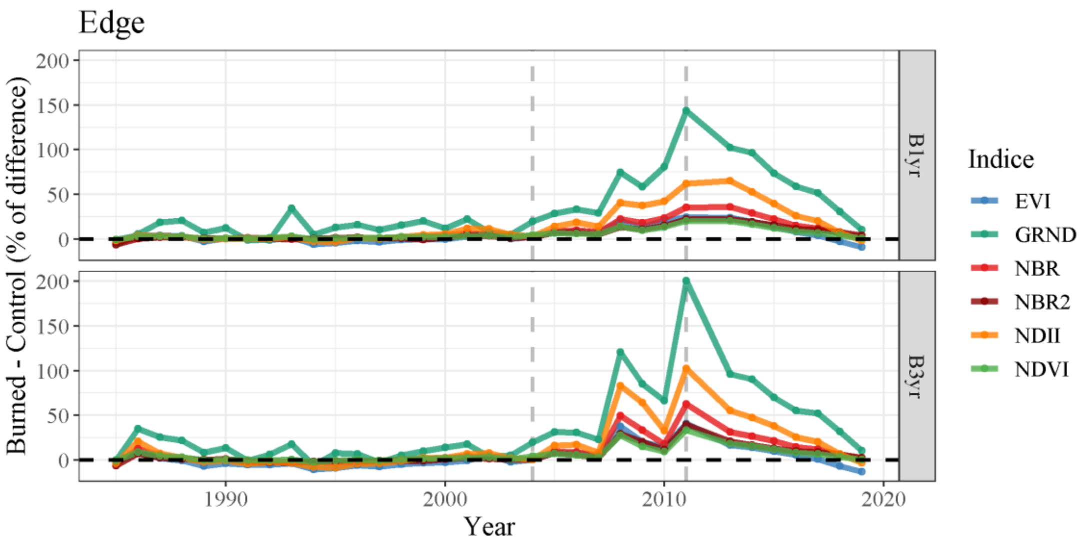

Figure S2. Relative difference in the means of the multispectral vegetation indices between the edges (<250 meters) of the treatments burned every three years (B3yr), burned annually (B1yr) and the edge of the control treatment. The values indicate the percentage difference in relation to the control treatment. The dashed lines indicate the years in which the experimental fires were conducted (2004 to 2010).

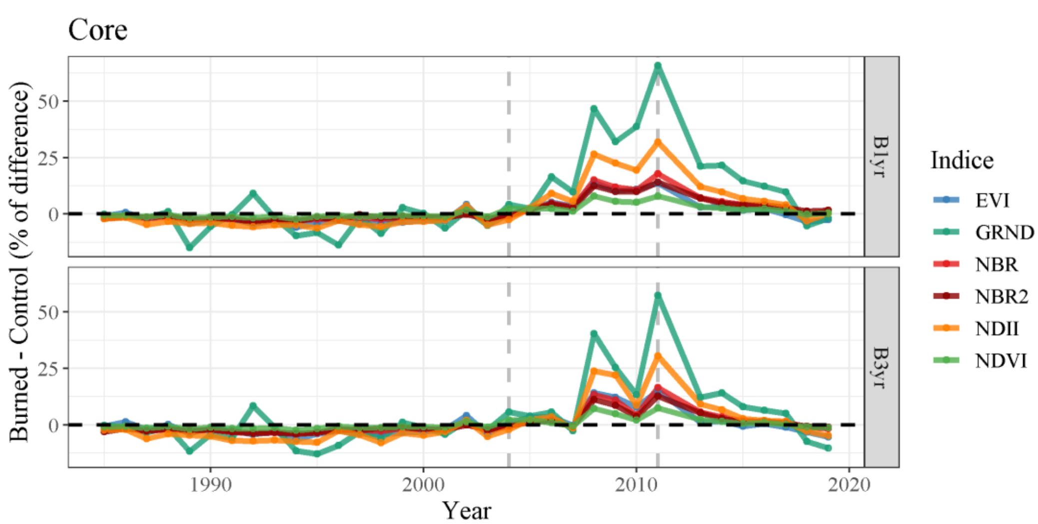

Figure S3. Relative difference in the means of the multispectral vegetation indices between the interior (>250 meters) of the plot treatments burned every three years (B3yr), burned annually (B1yr) and the interior of the control treatment. The values indicate the percentage difference in relation to the control treatment. The dashed lines indicate the years in which the experimental fires were conducted (2004 to 2010).

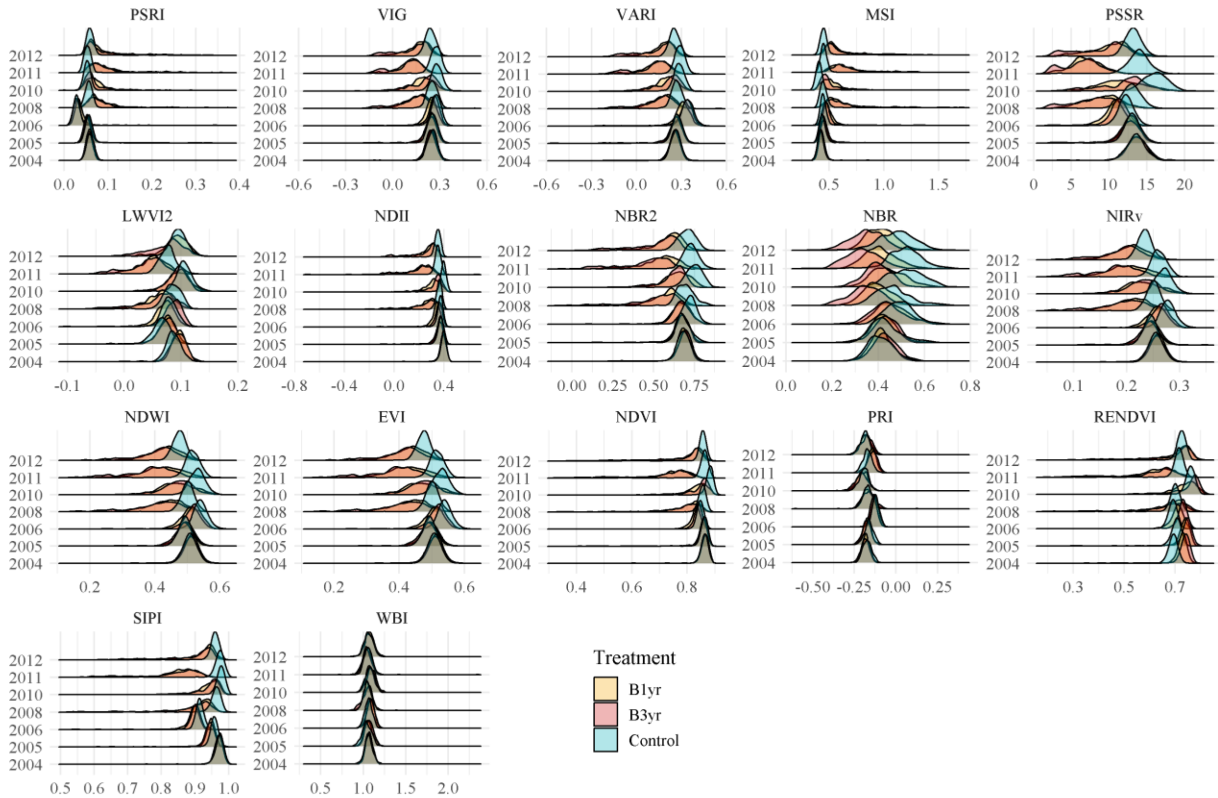

Figure S4. Distribution of Hyperion vegetation indices values throughout the fire experiment. The results are arranged in descending order from the vegetation indices that differed the most to those that differed least in relation to the control treatment.

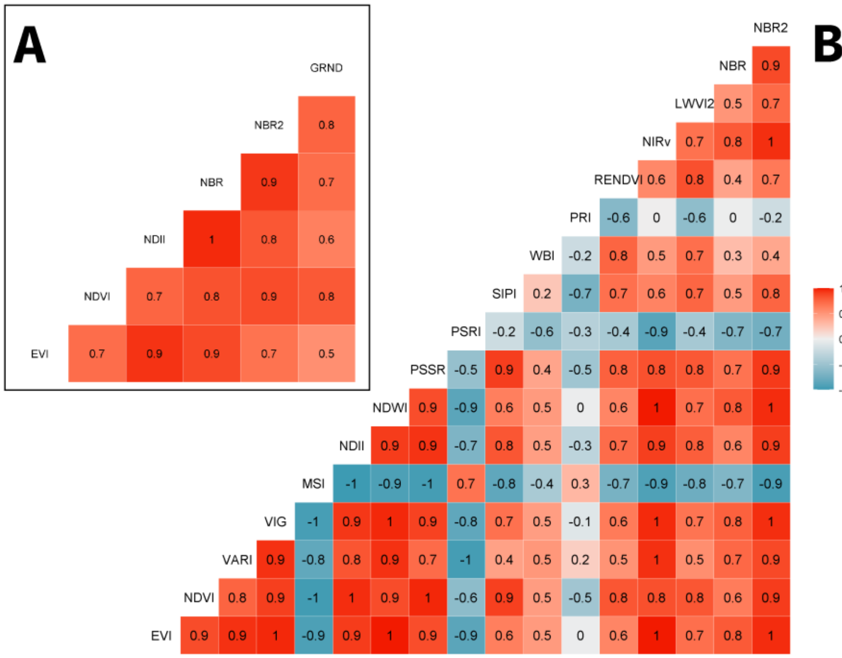

Figure S5. (A) Pearson's correlation matrix between the vegetation indices calculated using Landsat. (B) Pearson's correlation matrix between the vegetation indices calculated using the EO-1 (Hyperion).

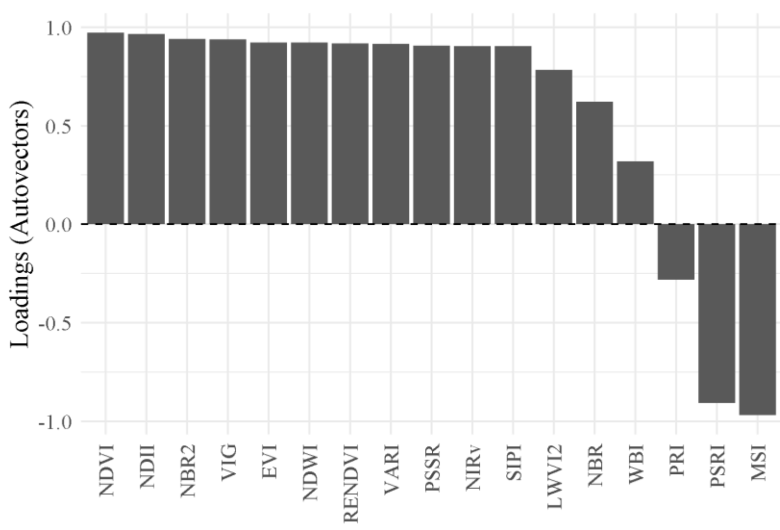

Figure S6. Component matrix values (eigenvectors) for the first principal component (PC1). PC1 was mainly driven by variations in the level of water stress and vegetation pigmentation of the burn treatments.

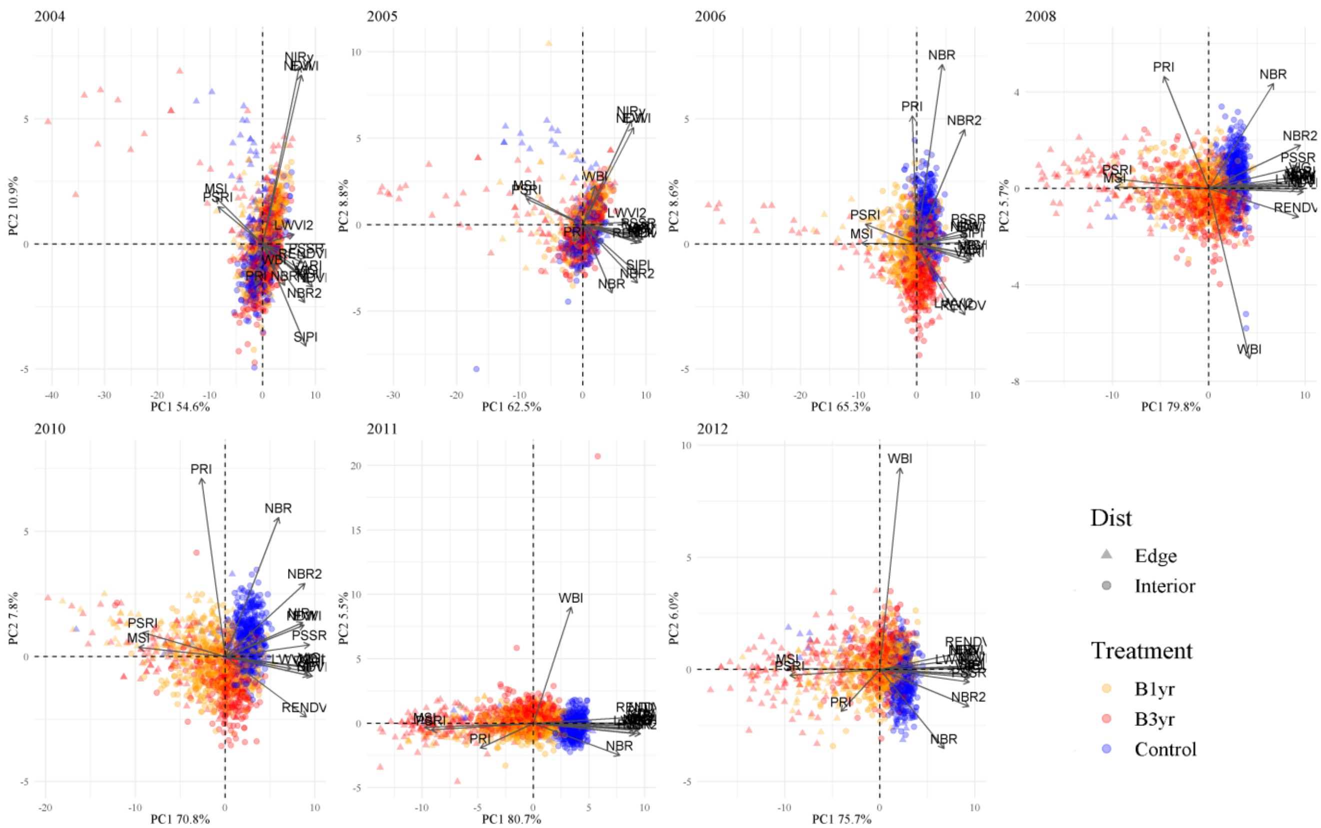

Figure S7. Projection of the first two principal components from the analysis applied to the values of the 17 VIs calculated using Hyperion data for all years of the time series. PCA discriminated the control treatment, triennial burn (B3yr) and annual burn (B1yr), which was affected by distance (Dist) from the edge.

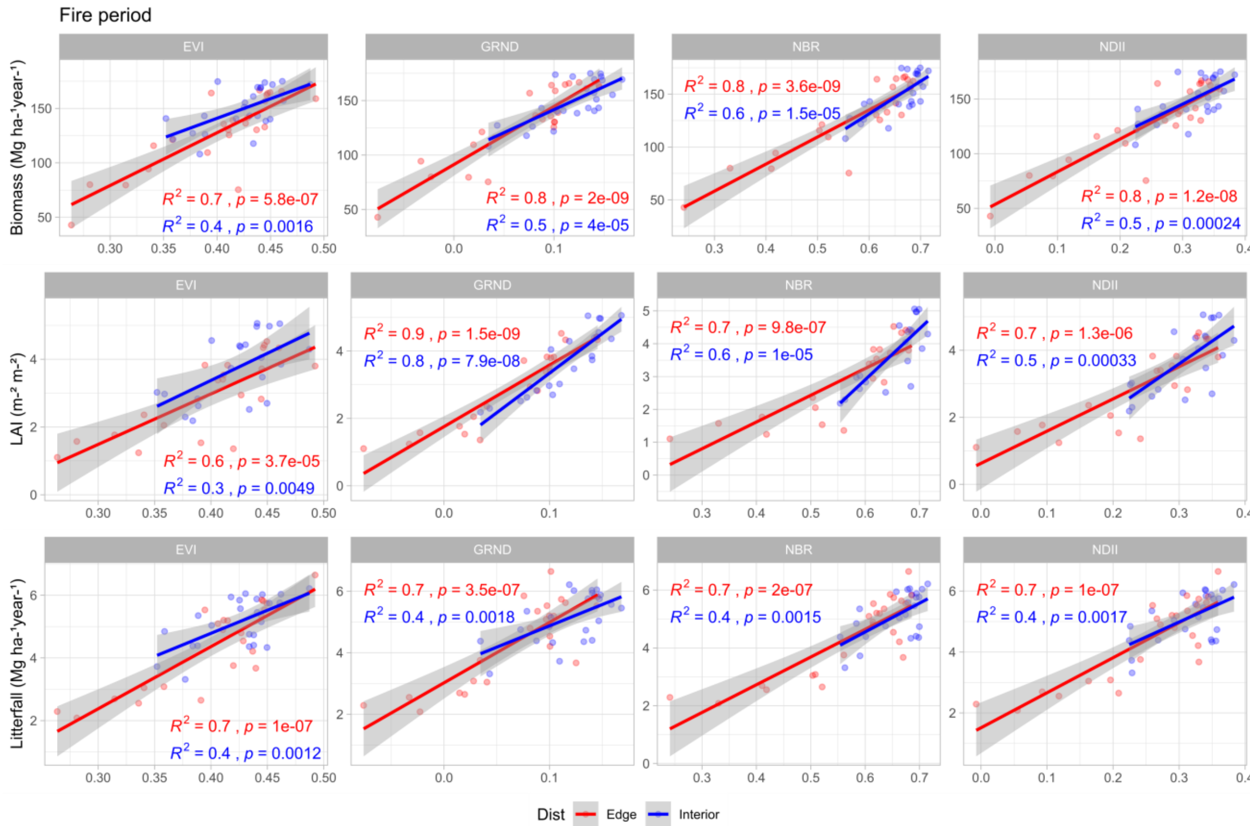

Figure S8. Linear model to evaluate how the VIs (Landsat) can explain in-situ information (Biomass, LAI, and Litterfall) during the experimental fire period (2004–2010). The analysis was segmented by forest edge (the first 250 m) and forest interior (250–1000 m). EVI = Enhanced Vegetation Index; GRND = Green Normalized Difference Vegetation Index; NIR = Near Infrared; NDII = Normalized Difference Infrared Index. The results in this figure show higher R^2 values at the forest edge, indicating that Landsat VIs can be used to evaluate forest degradation in Amazonia, especially at the edge and ecosystems experiencing high levels of disturbance.

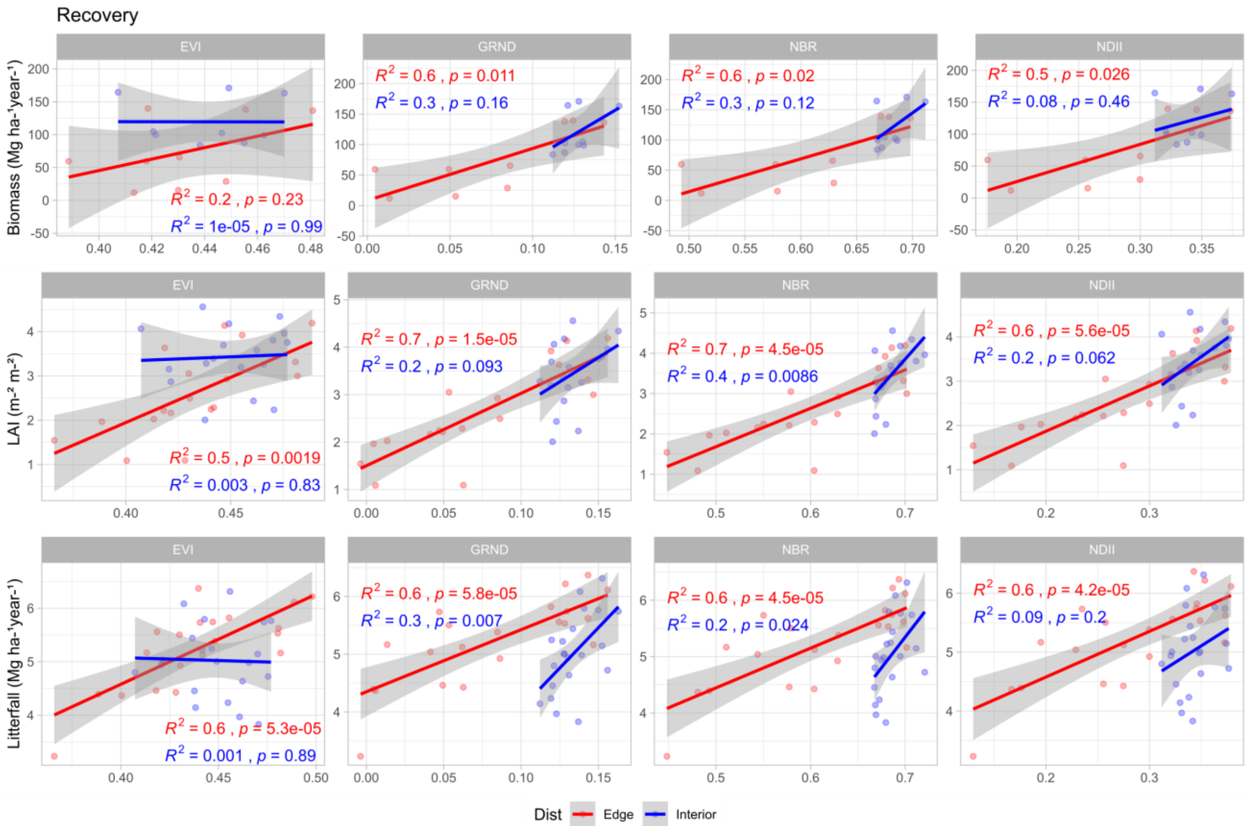

Figure S9. Linear model to evaluate how the VIs (Landsat) can explain in-situ information (Biomass, LAI, and Litterfall) during the fire recovery period (2011–2019). The analysis was segmented by forest edge (the first 250 m) and forest interior (250–1000 m). EVI = Enhanced Vegetation Index; GRND = Green Normalized Difference Vegetation Index; NIR = Near Infrared; NDII = Normalized Difference Infrared Index. The results in this figure reveal elevated R^2 values at the forest edge, suggesting that Landsat VIs are effective for assessing forest recovery in Amazonia, particularly at the forest edge and in ecosystems subjected to significant disturbance.

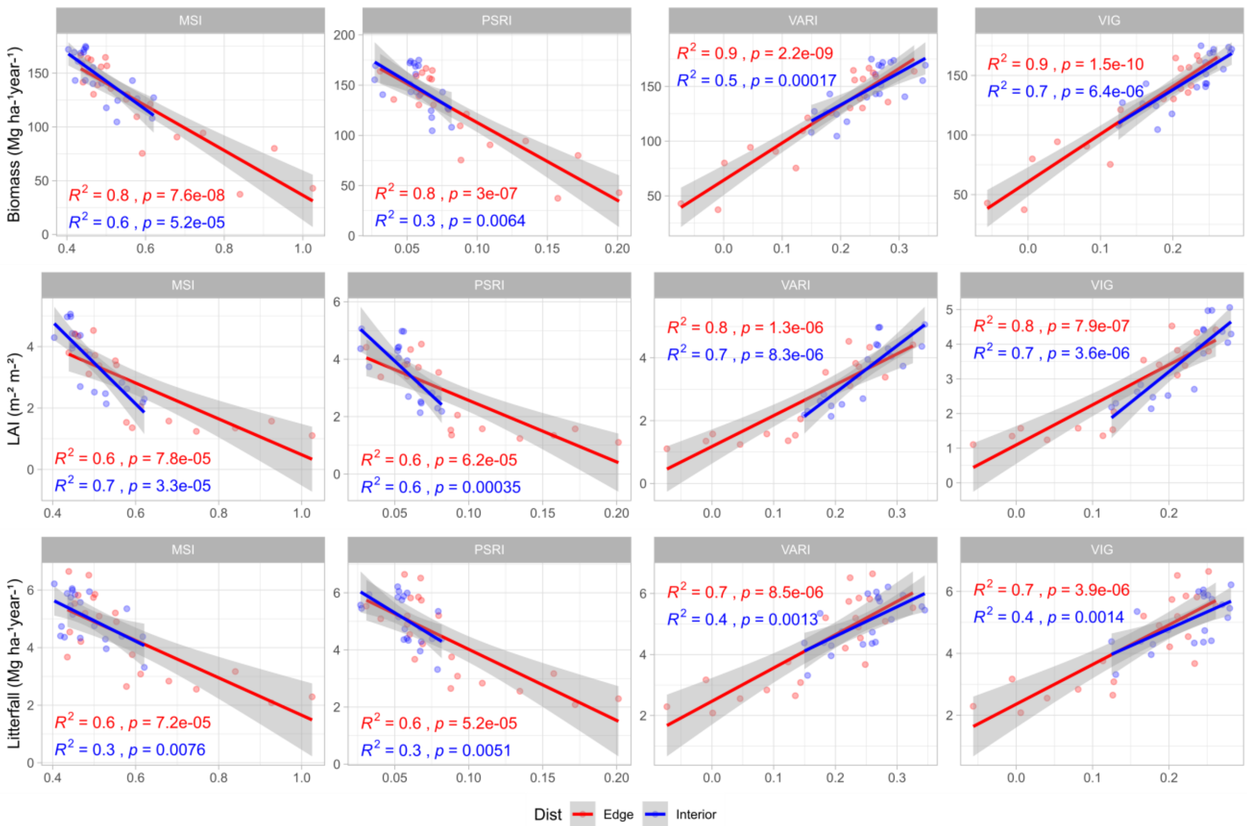

Figure S10. Linear model to evaluate how the VIs (Hyperion) can explain in-situ information (Biomass, LAI, and Litterfall) during entire time series of Hyperion dataset (2004 to 2012). The analysis was segmented by forest edge (the first 250 m) and forest interior (250–1000 m). MSI = Moisture Stress Index; PSRI = Plant Senescence Reflectance Index; VARI = Visible Atmospherically Resistant Index; VIG = Visible Index Green. The results in this figure show higher R^2 values at the forest edge, indicating that Landsat VIs can be used to evaluate forest degradation in Amazonia, especially at the edge and ecosystems experiencing high levels of disturbance.